# HIGH RESOLUTION WIND RETRIEVAL FOR SEAWINDS ON QUIKSCAT

**Jeremy B. Luke**
**Microwave Earth Remote Sensing Laboratory**
**Brigham Young University**
**Provo, Utah**
**May 5, 2003**

**Abstract**

The SeaWinds instrument was designed to provide wind measurements over the oceans with a resolution of 25x25 km per pixel. Through the use of image enhancement algorithms developed at BYU this resolution can be increased to as fine as 2.5x2.5 km. A description of key portions of this "high resolution" wind retrieval algorithm is given, with a summary of results.

## SYMBOLS

$\sigma^0$ = radar cross section
$\chi$ = relative wind direction
$P_t$ = power transmitted
$P_r$ = power received
$G$ = antenna gain
$A_{rs}$ = effective area of scatterer
$\lambda$ = wavelength of radiation
$R$ = distance from antenna to ocean surface
$U$ = wind speed
$\theta$ = incidence angle of radiation
$f$ = frequency of radiation
$pol$ = polarization of radiation

## INTRODUCTION

Wind over the ocean is the largest source of upper ocean momentum. Winds affect not only surface waves but also influence basin wide current systems. Winds also have a crucial role of modulating the air-sea fluxes of heat, gases, moisture, and particles which regulate regional and global climates. It is for these reasons that measurements of the wind over the ocean are becoming ever more important.

Conventionally measurements of the ocean winds were made by ships and buoys. These measurements cover only a very small part of the ocean surface. Ships generally follow trade routes and avoid bad storms making the measurements they take geographically and phenomenologically biased. Wind measurements made by ships are often inaccurate due to untrained observers, badly placed anemometers, and inadequate correction for ship velocity. Buoys, although very accurate, are few in number and generally close to land.

This limited coverage of the Earth's oceans was overcome with the launch of the first space-borne scatterometer. The Seasat-A Satellite Scatterometer (SASS) proved that the wind velocity over the ocean could accurately be measured from space during its operation from June to October of 1978. The SeaWinds scatterometer on QuikSCAT was launched June 19, 1999. This instrument is capable of measuring the wind velocity over 90 per cent of the ocean everyday.

The Seawinds instrument was designed to provide wind measurements with a resolution of 25x25 km per wind vector cell. The resolution of the wind measurements is increased, through exploitation of the of the SeaWinds measurement geometry and scatterometer image enhancement algorithms, to as fine as 2.5x2.5 km per wind vector cell. A description of key portions of the high resolution wind retrieval algorithm is given in this report.

## BACKGROUND

A scatterometer is an active remote sensing device. Scatterometers transmit pulses of electro-magnetic energy to the ocean surface and measure the amount of power reflected back to the sensor. From this power measurement an estimate of the radar cross section of the illuminated section of the ocean surface can be calculated. This estimate of $\sigma^0$ is given by the radar equation[1]

$$P_r = \frac{P_t G^2 \lambda^2 A_{rs} \sigma^0}{(4\pi)^3 R^4}. \quad (1)$$

The relationship between $\sigma^0$ and the ocean wind is given by the geophysical model function (GMF). The GMF is an empirically derived, multidimensional table. In its general form the GMF can be written as

$$\sigma^0 = \mathcal{M}(U, \chi, \theta, f, pol). \quad (2)$$

Illustrations of the GMF are given in Figures 1 and 2. From Figure 1 it can be seen that the relationship between $\sigma^0$ and the wind speed is linear with the log of the wind speed. This relationships shows that with one

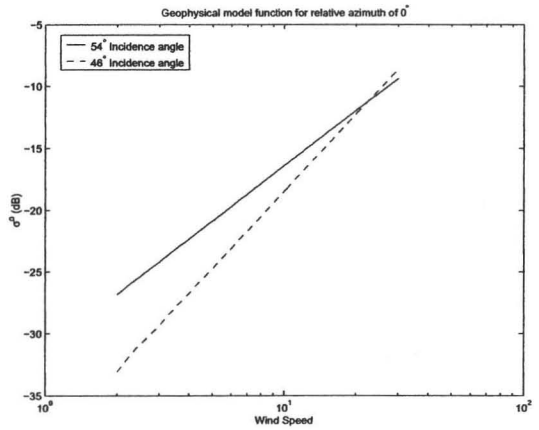


**Figure 1**: GMF relating wind speed to $\sigma^0$ with $\chi = 0°$. Incidence angles of 46° with horizontal polarization and 54° with vertical polarization were used to generate this plot.

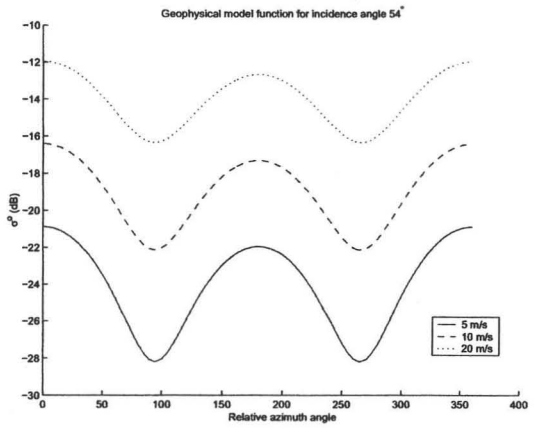


**Figure 2**: GMF relating relative azimuth angel to $\sigma^0$. Wind speeds of 5 m/s, 10 m/s, and 20 m/s with an incidence angle of 54° were used to generate this plot from the "Wentz" model[3] function.

$\sigma^0$ measurement a good estimate of the wind speed can be made. The wind direction however does not have a linear relationship with $\sigma^0$. The relationship between $\sigma^0$ and wind direction is given by[1]

$$\sigma^0(\chi) = A_0 + A_1 cos(\chi) + A_2 cos(2\chi) \qquad (3)$$

where $A_0$, $A_1$, and $A_2$ are dependent on incidence angle, polarization and wind speed. This azimuth variation in $\sigma^0$ is maximum when the radar look direction is upwind. A slightly lower maximum occurs when the radar look direction is downwind. The minimums in Equation 3 occur when the radar look direction is perpendicular to the wind direction. This relationship between $\sigma^0$ and $\chi$ is shown in Figure 2. Determining wind direction from one $\sigma^0$ measurement is not possible, however wind direction can be estimated when multiple $\sigma^0$ measurements are made from a variety of azimuth and incidence angles. This process is illustrated in Figure 3. Here each curve represents all of the possible wind speeds and directions that can produce the same $\sigma^0$. It can be seen that with only one $\sigma^0$ measurement it is not possible to uniquely determine the wind speed and direction. If a second $\sigma^0$ measurement is made of the same section of ocean from a different azimuth angle and/or incidence angle then the possible wind speeds and directions can be narrowed down to the intersection of the two curves. Figure 3 shows four curves each representing a $\sigma^0$ measurement of the section of ocean made from unique azimuth and incidence angles. The one intersection corresponds to the wind speed and direction that produced the $\sigma^0$ measurements.

Noise in the $\sigma^0$ measurements in effect causes the curves shown in Figure 3 to be shifted up or down.

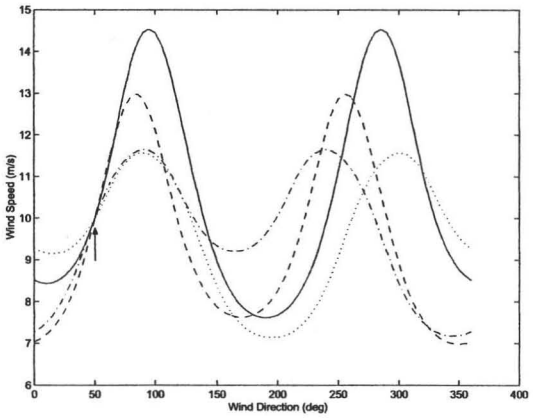


**Figure 3**: Each curve represents the possible wind vectors for a given $\sigma^0$ measurement. Four curves are shown each corresponding to a unique $\sigma^0$ measurement of a given area made from a unique azimuth angle and incident angle. The intersection of the four plots is the wind speed and direction.

This noise can make near intersections to be mistaken for the true intersection of the $\sigma^0$ curves. The wind retrieval algorithm is thus forced to report near intersections as possible wind vector solutions for a given set of $\sigma^0$ measurements. These possible solutions are known as ambiguities.

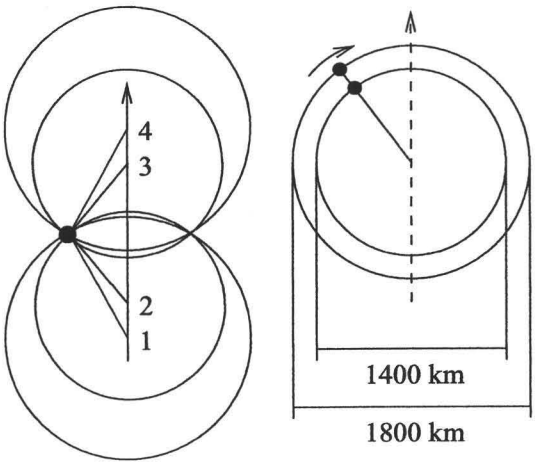


**Figure 4**: (a) The Seawinds scatterometer is capable of viewing an area in the inner swath four times. Both the inner and outer beam view the area looking forward and then again looking in the aft direction. (b) The SeaWinds instrument has a swath width of 1400 km for the inner beam and 1800 km for the outer beam.

## SeaWinds Scatterometer

The SeaWinds instrument is a conically scanning dual pencil beam scatterometer. SeaWinds operates at a frequency of 13.4 GHz. The inner beam has an incidence angle of 46°with horizontal polarization while the outer beam with an incidence angle of 54°uses vertical polarization. With this geometry the SeaWinds instrument is capable of measuring the radar cross section of a small area of ocean four times from different azimuth angles at the two incidence angles. Two of the measurements are made by the scatterometer looking forward, one with each beam. Two more are made after the satellite passes the area with the two beams looking in the aft direction. The QuikSCAT satellite orbits the Earth in circular, sun-synchronous orbit at a height of 803 km. The swath width for the outer beam is 1800 km and the swath width of the inner beam is 1400 km. The SeaWinds instrument has a radar pulse repetition frequency (PRF) of 187.5 Hz and an antenna spin rate of 18 RPM. This provides overlap in the illuminated area from which sequential $\sigma^0$ measurements are made. The SeaWinds instrument produces two $\sigma^0$ measurement types. The first type uses the power returned form the entire illuminated area. This measurement is known as an "egg". The second type uses range and Doppler filtering to resolve the power returned from smaller sections of the illuminated

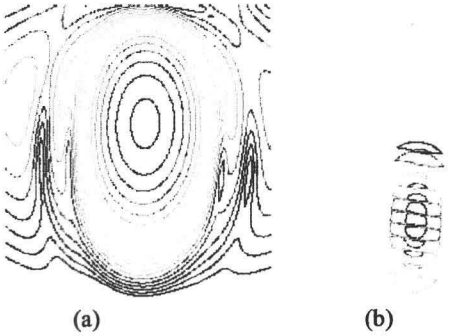


**Figure 5**: Contour plot of the $\sigma^0$ measurement response for (a) eggs and (b) slices. The contour interval is 3dB. Shown in (b) are twelve slices however data received from JPL contains information on the inner eight slices. Image courtesy of Dr. David Long

area. Because these measurements appear to slice up the illuminated area they are known as slices. The SeaWinds illumination pattern is shown in Figure 5 (a). The power reflected from the area illuminated by the 6 dB contour is used in the calculation of $\sigma^0$. The area of an egg is an ellipse, approximately 25 km in the azimuth direction and 37 km in the look direction. Figure 5 (b) shows a comparison of the slice area. Slices have a length that is commandable in the look direction from 2-10km with a length of approximately 25 km in the azimuth direction.

Currently the wind product produced by the Jet Propulsion Laboratory (JPL) from SeaWinds has a resolution that is 25x25 km. This product uses the egg $\sigma^0$ measurements. These measurements are gridded into 25x25 km cells known as wind vector cells (WVC). If the center of the egg measurement falls within the area of a WVC it is used in the calculation of the wind in that WVC. If part of the area illuminated by an egg measurement is over land the wind is not retrieved for that WVC. This limits how close to land winds can be reported.

## High Resolution Winds

By taking advantage of the overlap in $\sigma^0$ measurements due to both the PRF and antenna spin rate along with the overlap due to the velocity of the satellite, high resolution $\sigma^0$ fields can be made. These high resolution $\sigma^0$ fields are generated by applying the AVE$^2$ algorithm. Four $\sigma^0$ fields are made for each beam, inner-forward looking, inner-aft looking, outer-forward looking, and outer-aft looking, of the entire revolution of the QuikSCAT satellite. The resolution of these $\sigma^0$ fields is 2.5 x2.5 km. This data is then passed to the wind retrieval algorithm.

The wind fields generated by these high resolution $\sigma^0$ fields are reported at the same resolution as the

$\sigma^0$ fields. The high resolution wind measurements are however noisier than are the lower resolution winds reported by JPL.

## COMPOSITING KP

High resolution wind retrieval requires that several parameters be composited. The most important of these is the $\sigma^0$ measurement. This compositing is done, as previously mentioned, using the AVE algorithm. To increase the accuracy of the high resolution winds the parameter known as $K_p$ also needs to be composited. $K_p$ is defined to be the normalized standard deviation of $\sigma^0$. It is given by

$$K_p = \frac{\sqrt{\text{var}[\sigma^0]}}{E[\sigma^0]} \tag{4}$$

where $var[\,]$ is the variance and $E[\,]$ is the expectation operator. Kp is used in the estimation of the wind from the set of $\sigma^0$ measurements. The goal therefore is to derive a method to composite $K_p$ for slices into $K_p$ for eggs. To do this a method for compositing $\sigma^0$ must be derived. This is done by realizing that the power in the egg measurement is the sum of the power in the slice measurements i.e.

$$P_e = \sum_i P_{s,i}. \tag{5}$$

This can be written in terms of $\sigma^0$ if we rewrite Equation 1 as

$$\begin{aligned} P_r &= X\sigma^0 & (6)\\ \sigma_e^0 X_e &= \sum_i \sigma_i^0 X_{s,i}. & (7) \end{aligned}$$

The $X$ variable is known as the X factor and is recorded with the satellite data. The X factor for the egg measurement is approximately equal to the sum of the slice X factors. With this the compositing equation for the egg $\sigma^0$ is given by

$$\sigma_e^0 = \frac{\sum_{i=1}^{n} \sigma_{s,i}^0 X_{s,i}}{\sum_{i=1}^{n} X_{s,i}}. \tag{8}$$

The derivation of the compositing method for $K_p$ uses a similar approach. The first step is to find the variance of the egg $\sigma^0$ in terms of the power in each slice,

$$\begin{aligned} \text{var}[\sigma_e^0] &= E[(\sigma_e^0)^2] - E[\sigma_e^0]^2 \\ &= E\left[\left(\frac{P_e}{X_e}\right)^2\right] - E\left[\frac{P_e}{X_e}\right]^2 \\ &= E\left[\left(\frac{\sum_i P_{s,i}}{\sum_i X_{s,i}}\right)^2\right] - E\left[\frac{\sum_i P_{s,i}}{\sum_i X_{s,i}}\right]^2 \\ &= \frac{\sum_i \sum_j E[P_{s,i}P_{s,j}]}{\left(\sum_i X_{s,i}\right)^2} - \left(\frac{\sum_i E[P_{s,i}]^2}{\sum_i X_{s,i}}\right). \end{aligned} \tag{9}$$

A model[4] for the noise in the $\sigma^0$ measurement with the substitution of Equation 6 can be written in terms of the power in each slice i.e.

$$\begin{aligned} \sigma_{s,i}^0 &= \sigma_t^0(1 + K_{pi}\nu_i) \\ \frac{P_{s,i}}{X_{s,i}} &= \sigma_t^0(1 + K_{pi}\nu_i) \\ P_{s,i} &= \sigma_t^0 X_{s,i}(1 + K_{pi}\nu_i). & (10) \end{aligned}$$

where $\sigma_t^0$ is the true $\sigma^0$ and $\nu_i$ is a Gaussian white random variable. Using Equation 10 and the fact that $\nu$ is uncorrelated the variance and mean of $\sigma^0$ can now be written as

$$\text{var}[\sigma_e^0] = (\sigma_t^0)^2 \frac{\sum_i X_{s,i}^2 K_{p,i}^2}{\left(\sum_i X_{s,i}\right)^2} \tag{11}$$

$$E[\sigma_e^0] = \frac{\sum_i \sigma_t^0 X_{s,i}}{\sum_i X_{s,i}} = \sigma_t^0. \tag{12}$$

The compositing method for $K_p$ is then found by plugging Equations 11 and 12 into equation 4,

$$K_p^2 = \frac{\sum_i X_{s,i}^2 K_{p,i}^2}{\left(\sum_i X_{s,i}\right)^2}. \tag{13}$$

A second method for compositing $K_p$ is derived using the parameter of $K_p$ recorded in the data files. $K_p$ can be written in terms of these parameters,

$$K_p^2 = A + \frac{B}{SNR} + \frac{C}{SNR^2}. \tag{14}$$

This method first composites the $A$, $B$, and $C$ parameters along with the $SNR$ from the slices to get a composite $K_p$. The compositing equations are

$$A_{comp} = \frac{\sum_i X_{s,i}^2 A_i^s}{\left(\sum_i X_{s,i}\right)^2} \tag{15}$$

$$B_{comp} = \frac{B^s}{N} \tag{16}$$

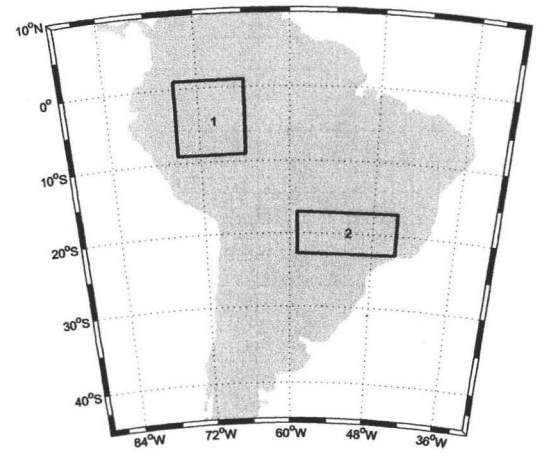


(a)

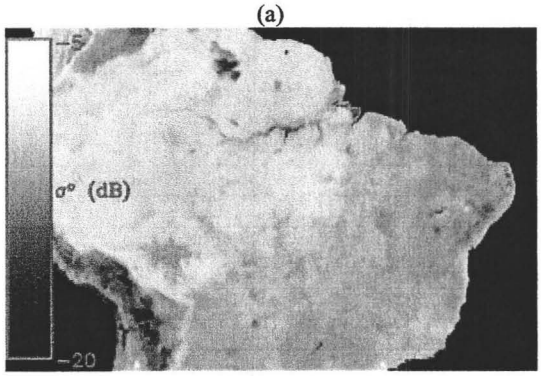


(b)

**Figure 6**: (a) Regions of homogeneous backscatter used in study. (b) SIR images showing backscatter. (quev-a-Ama01-257-260.sir)

$$C_{comp} = \frac{C^s}{N} \tag{17}$$

$$SNR_{comp} = \frac{\sum_i SNR_i^s X_{s,i}}{\sum_i X_{s,i}}. \tag{18}$$

## Verification

To verify the $K_p$ composing methods two regions of semi-homogeneous $\sigma^0$ are used. The $\sigma^0$ from these regions is used to compute and empirical $K_p$ value which is then compared to the egg $K_p$ and the composite $K_p$ using both methods. Both perform similarly, producing values that are slightly higher than is the egg $K_p$. The empirical value of $K_p$ in the study region is higher than is the value of $K_p$ for eggs and composite slices. The higher value in the empirical $K_p$ is due to variability in the radar cross section of the land itself.

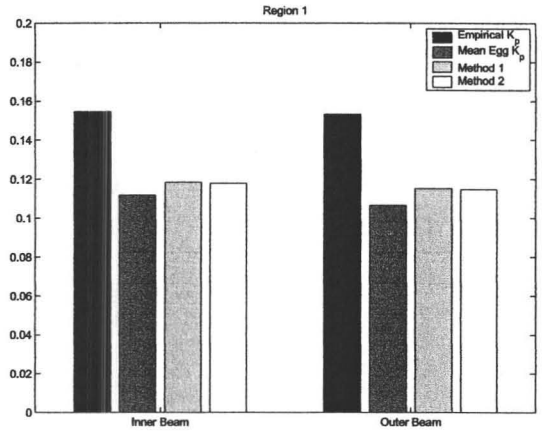


(a)

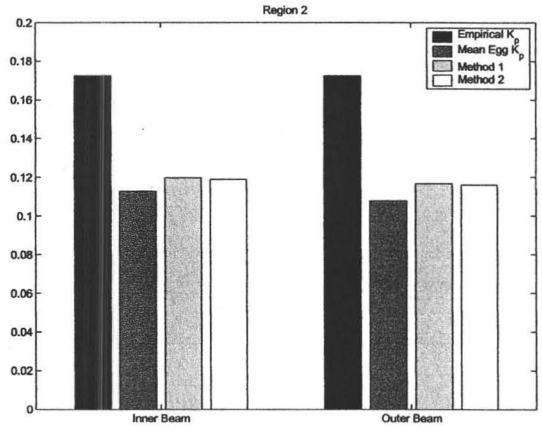


(b)

**Figure 7**: $K_p$ values for both regions in Figure 6. The results of method 1 and 2 for compositing $K_p$. The number of measurements for each region and beam are: Region 1 inner beam 25,024, outer beam 23,166, Region 2 inner beam 12,320, and outer beam 12,765

## AMBIGUITY SELECTION

One of the difficulties in wind retrieval is selecting the ambiguity closest to the true wind vector. For scatterometers with good instrument skill the ambiguity with the highest likelihood is generally the ambiguity closest to the true wind. The most likely ambiguity is referred to as the first ambiguity. These scatterometers can then make a good initial guess by selecting the first ambiguity. The SeaWinds instrument does in fact have good instrument skill in the "sweet spot" of the swath, however this instrument skill is lost when the resolution enhancement algorithms are performed on the data. An ambiguity se-

lection algorithm must be adapted for the high resolution wind fields.

A widely used ambiguity selection algorithm is a median filter based technique. This algorithm requires that the wind field be initialized. The method used to initialize the high resolution wind field is to choose the ambiguity closest the that chosen in low resolution wind reported by JPL.

The ambiguity selection algorithm chooses the ambiguity that minimizes the error with the surrounding winds. The selected ambiguity at cell $(i, j)$ is given by

$$\hat{\mathbf{w}} = \arg\min_{k} \sum_{n=j-L}^{j+L} \sum_{m=j-L}^{j+L} \|\mathbf{w}_{mn}^{k} - \mathbf{v}_{mn}\| \qquad (19)$$

where $\mathbf{v}_{mn}$ represents the wind vector at cell $(m, n)$, $k$ is the index of the ambiguities, and $L$ specifies the size of the filter.

The size of the filter is an important parameter in the high resolution wind retrieval. For every pixel in the low resolution wind image there are 100 high resolution pixels. Initialization of the high resolution wind field with the low resolution can introduce errors if the wind velocity changes within the 25x25 km low resolution pixel. Also, an incorrectly selected low resolution ambiguity causes 100 high resolution pixels to be initialized with the incorrect wind. The size of the filter thus needs to be large enough to correct for this.

A study region from revolution 14209 of the QuikSCAT satellite is chosen to analyze the correct filter size. The region is located in the South Pacific off the coast of Chile. Figure 8 illustrates the wind flow in this area. The high resolution wind speed and direction after initialization are shown in Figures 9 and 10. Problems with this initialization are evident in the wind direction image. Along the wind front in the left side of the image the transition between wind directions is coarse. Through the use of the ambiguity selection algorithm this front is filtered to be more realistic. Also isolated squares of incorrect wind speed are evident in the images these are also eliminated through the use of the ambiguity selection algorithm.

Several filter sizes were tested to subjectively choose the one that performed the best. Filter sizes of 3x3 and 5x5 did not completely remove the coarseness of the images. The 7x7 filter (results shown in Figures 11 and 12) performed well removing most of the bad initializations. Larger size filters were also examined but improvements beyond the 7x7 filter are minimal.

The other consideration in choosing the filter size increased computation time. For the study region the ambiguity selection program was timed, results are shown in Table 1. The 7x7 filter has the best performance and for this reason is the size chosen for the high resolution wind retrieval algorithm.

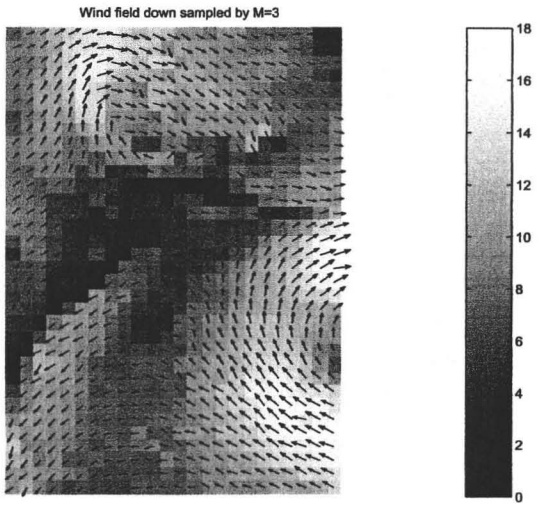


**Figure 8**: Selected study area. Background color is wind speed in meters per second. The images is created from low resolution data down sampled.

**Table 1**: Comparison in processing time for each filter size. Processing time is given in minutes and seconds.

| Filter Size | Iterations | Processing Time |
|---|---|---|
| 3x3 | 17 | 1:06.92 |
| 5x5 | 65 | 4:47.41 |
| 7x7 | 87 | 11:05.24 |
| 11x11 | 100 | 28:06.4 |

## CONCLUSION

The high resolution wind retrieval algorithm increases the resolution of the winds estimated from data produces by the SeaWinds instrument from 25x25 km per pixel to 2.5x2.5 km. This resolution enhancement is beneficial for at least two reasons. First the high resolution wind retrieval algorithm allows wind to be retrieved close to land. The second is better storm tracking. The high resolution wind retrieval algorithm can resolve the eye of hurricanes.[5]

The compositing formulas for $K_p$ shown in this paper increase the accuracy of the retrieved high resolution winds. Ambiguity selection is performed in the high resolution winds by applying a median filter based technique. A filter size of 7x7 is subjectively shown to have the best performance and is therefor the size used in the high resolution wind retrieval algorithm.

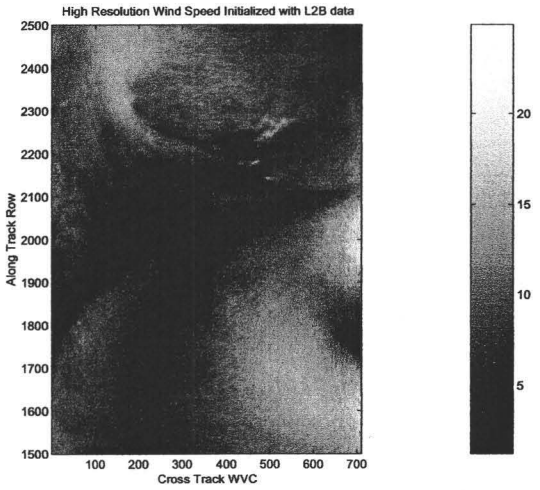


**Figure 9**: High resolution wind speed in study area initialized with low resolution wind field.

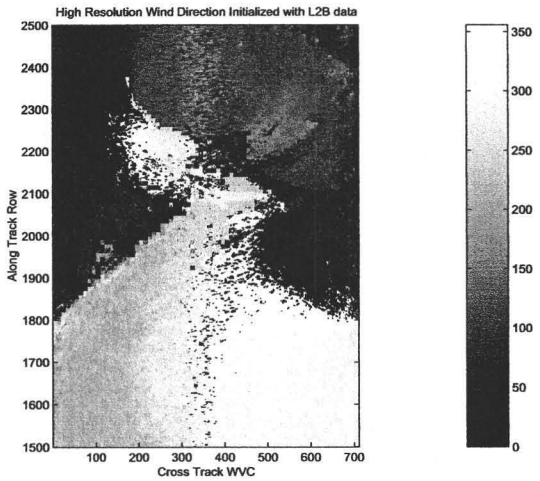


**Figure 10**: High resolution wind direction in study area initialized with low resolution wind field.

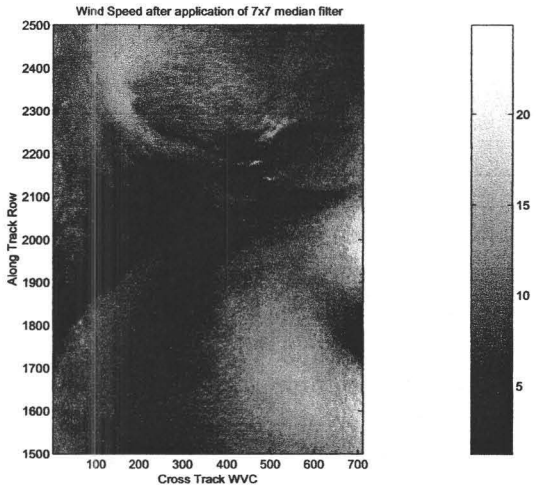


**Figure 11**: High resolution wind speed in study area after application of 7x7 median filter based ambiguity selection algorithm.

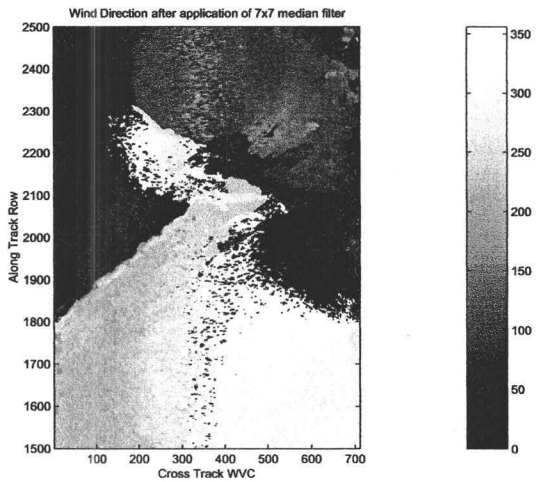


**Figure 12**: High resolution wind direction in study area after application of 7x7 median filter based ambiguity selection algorithm.

## References


[1] F. T. Ulaby, R. K. Moore, A. K. Fung, *Microwave Remote Sensing Active and Passive, vol. 2*, Artech House, MA, 1986.

[2] D.G. Long, P. Hardin, and P.T. Whiting, "Resolution Enhancement of Spaceborne Scatterometer Data," *IEEE Transactions on Geoscience and Remote Sensing*, vol. 32, no. 3, pp. 700-715, 1993.

[3] F.J. Wentz, L.A. Mattox, S. Peteherych, "A Model Function for Ocean Radar Cross Sections at 14.6 GHz," *Journal of Geophysical Research*, vol. 89, pp. 3689-3704, 1984

[4] T.E. Oliphant, D.G. Long, "Accuracy of Scatterometer-Derived Winds using the Cramer-Rao Bound," *IEEE Transactions on Geoscience and Remote Sensing*, vol. 37, no. 6, Nov 1999

[5] D.G. Long, "High Resolution Wind Retrieval from SeaWinds," *International Geoscience and Remote Sensing Symposium*, vol. 2, pp. 751-753, June 2002.